Estimation of Rician Channels From Indoor Measurements at 26 GHz

Nielsen, Jesper Ødum; Pedersen, Gert F.

Published in:
The 29th Annual IEEE International Symposium on Personal, Indoor and Mobile Radio Communications (IEEE PIMRC 2018)

DOI (link to publication from Publisher):
10.1109/PIMRC.2018.8580975

Publication date:
2018

Estimation of Rician Channels From Indoor Measurements at 26 GHz

Jesper Ødum Nielsen, Gert Frølund Pedersen

APMS, Dept. of Electronic Systems, Technical Faculty of IT and Design, Aalborg University, Denmark

***Abstract*—The aim of this work is to evaluate amplitude distributions of narrow-band channels based on sounding measurements made at 26 GHz. The setup is with an omni-directional antenna moving in different indoor environments with an access point (AP). Rician channel model parameters are obtained via maximum likelihood (ML) estimation and the k-factors are obtained as well as mean power levels. Depending on the type of environment and the location of the mobile with respect to the used AP, the found k-factors varies from about -10 dB up to about 9 dB.**

I. Introduction

With the aim of supporting an increased network capacity and speeds, future communication systems like 5G are expected to utilize frequency spectrum at much higher frequencies than the typically below 6 GHz used in today's systems. Frequencies near 28 GHz have been considered attractive due to available spectrum and expected reasonable propagation conditions [1].

So far only relatively few publications exist that are based on measurements of the radio channel in this band, *e.g.*, [2], yet the radio propagation in the new band is expected to be very different from that in legacy bands where many works exist. Hence new empirical results are required to quantify the properties of the new type of channels. The current work focuses on the amplitude distribution of a moving mobile station being served by an AP in an indoor environment. Related previous works include [3], [4] for bands about 30 GHz and [5] about 60 GHz.

II. Channel Measurements

A. Setup

The measurements used in the current work were obtained as part of a campaign previously described in [6], but the particular data needed for the analyses of the current work was not processed in [6]. The below text describes the measurements obtained with the channel sounder, with emphasis on the data used in the current work.

The sounder is configured to have one Tx channel (with either vertical polarization (VP) or horizontal polarization (HP), see below) and five Rx channels. The bandwidth is about 100 MHz and centered at 26 GHz. Each channel snapshot last 41 μs and the channel snapshot rate is 90 Hz, allowing fast azimuthal sweeps, as described below.

TABLE I
Overview of Tx horn orientations.

Env.	Tx Orient.	Description
Lab	O1	Towards Rx, South
	O2	66° from Rx dir., South-East
Corr	O3	Towards Rx along corridor, North
	O4	48° from Rx dir., North-West
Hall	O1	Towards Rx, West
	O2	66° from Rx dir., towards South-West
	O4	48° from Rx dir., towards North-West

The single Tx antenna was a linearly polarized 10 dB standard gain horn antenna (Pasternack PE9851/2F-10) which has a 3 dB beamwidth of 54° and 53° in the E- and H-plane, respectively. The Tx horn was mounted on a wooden mast 2.07 m above the floor, mimicking an access point in an indoor radio network. The horn was manually rotated, so that the Tx had either VP or HP. As described further below, three different locations of the Tx mast were used, one for each of the Lab, Corr, and Hall environments. For each location, 2-3 azimuthal orientations of the horn were used, as described in Table I.

At the Rx end of the sounder, four horn antennas and one omni-directional antenna were mounted on a pedestal which can rotate in azimuth, controlled by software in synchronicity with the channel sounding. Only data from the omni-directional antenna are used in the current work.

The omni-directional antenna (AINFO SZ-2003000/P) was mounted on top of the horns with the antenna center at a horizontal distance of 0.165 m from the rotation center and 1.0 m above the floor. During a measurement, the pedestal rotated 180° in azimuth, so that the antenna was moved along a half-circle path of length 0.52 m or about 45 wavelengths. The pedestal with the antennas mounted are shown left in Fig. 1. A single scan lasted about 2.9 s, during which time 525 channel snapshots were obtained from the omni-directional antenna.

B. Measurement Series

For each combination of location and orientation of the Tx horn and the Rx pedestal, two measurements were

Accepted for *The 2018 IEEE 29th Annual International Symposium on Personal, Indoor and Mobile Radio Communications (PIMRC).*

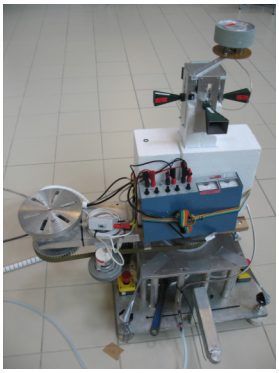

Fig. 1. Left: The pedestal with four horn antennas (three visible) and one omni-directional antenna mounted. Right: The corridor environment.

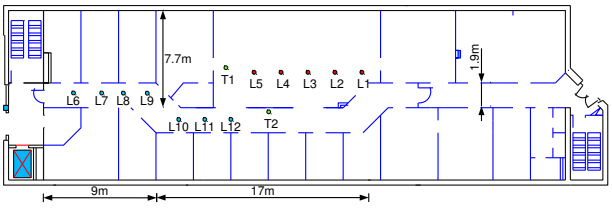

Fig. 2. Sketch of the Lab and Corr environments, including Tx and Rx locations.

Fig. 3. The laboratory environment.

carried out; one with the Tx horn configured for VP, and one with the Tx horn configured for HP. This allows a characterization of all four possible combinations of channels when transmitting and receiving in one of the two polarizations. However, in the current work only data resulting from using the VP of the Tx horn is utilized, since the omni-directional Rx antenna has VP and the cross-polarization coupling in the channel is low, leading to a generally unsatisfactorily measurement quality. Results on cross-coupling in the channel, obtained using the horn antennas, may be found in [6].

Below a few measurement series are defined by the location and orientation of the Tx and Rx in a given overall environment. In each case, the Tx location was fixed, but with a few different orientations. The pedestal with the Rx was moved to different locations in order to induce large-scale changes in the channel, with changes in both propagation path lengths and angles. The Rx locations are described below with the notation "Ln", where n is an integer number.

In order to also allow investigation of channel changes due to small-scale changes in the location, for each large-scale location four *sub-locations* are defined by the corners of a 10 cm by 10 cm square. Measurements were carried out at each of the sub-locations, except for some of the Hall series. In addition, some measurements were repeated.

In the campaign, four different measurement series were carried out, as described below

1) Lab: The Tx was located at the end of the laboratory environment, shown as T1 in Fig. 2, while the Rx pedestal was in five overall locations, L1, L2, ..., L5. For each of those locations, four sub-locations were used. Two orientations of the Tx were used, one directly towards the Rx (South) and one with the horn main direction partly towards the East wall of the lab. The lab environment is shown in Fig. 3.

2) Corr: The Tx was located near the wall in the corridor outside the laboratory, shown as T2 in Fig. 2. The Rx pedestal was in seven overall locations distributed along the corridor, of which L10, L11, L12 were in line of sight (LOS) from the Tx. Locations L6, L7, L8, L9 are in non line of sight (NLOS) since there is a bend in the corridor. The Tx was oriented both along the corridor as well as with the main direction partly towards the West corridor wall. The corridor is seen to the right in Fig. 1.

3) Hall: The Tx was located near one of the pillars in the East side of the Hall, below the overhanging first floor, see T3 in Fig. 4 and Fig. 5. The Rx pedestal was located at seven overall locations distributed along a radial line, shown in the sketch as L13, L14, ..., L19, all of which were in LOS from the Tx. Two orientations of the Tx were used, one directly towards the Rx and one where the horn main direction points partly towards the North wall.

In a second part of the Hall series of measurements, the Rx pedestal was located at the seven locations L19, L20,..., L25, distributed along an North-South line. For those locations both the length and angle of the LOS varies. Three orientations of the Tx were used, with the horn main direction pointing towards West, North-West, and South-West, thus focusing on different parts of of the hall.

Note that in the previous work [6] the two parts of the Hall series were treated separately, but are presented together here for simplicity.

III. Data Processing

A Rician channel is characterized by a specular component $s_s(t)$ and a zero-mean Gaussian distributed

Accepted for *The 2018 IEEE 29th Annual International Symposium on Personal, Indoor and Mobile Radio Communications (PIMRC).*

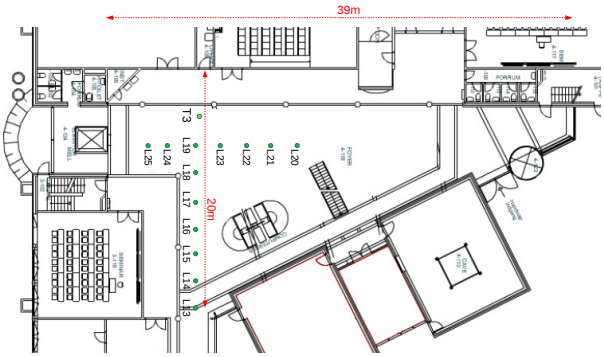

Fig. 4. Sketch of the Hall environment including Tx and Rx locations.

Fig. 5. The hall environment with the Tx visible on the left and the Rx pedestal in front of the stairs to the right.

random component $s_r(t)$, both complex. The received signal is the sum of the two components, so that the observed signal is

$$r(t) = s_s(t) + s_r(t) \tag{1}$$

in noise-less conditions. The amplitude $|r(t)|$ is Rician distributed [7]. Conventionally, the Rician channel is described by the k-factor defined as

$$k = 10 \log_{10} \left(\frac{\sigma_s^2}{2\,\sigma_r^2} \right) \tag{2}$$

in dB and where σ_s^2 and σ_r^2 are the power in the specular and random components, respectively. The k-factor is convenient since it in one figure describes the degree of randomness when a stable specular component is also present.

When dealing with measurements we only have access to a noise contaminated version of the amplitude, $r'(t) = r(t) + w(t)$, where $w(t)$ is the added noise. Assuming the channel is correctly described by the Rician model, the task is to estimate σ_s^2 and σ_r^2 from the noisy measurement. In this work the ML approach is used to estimate the Rice distribution parameters, since it outperforms the often used so-called method of moments [8]. Specifically, the ML estimation implementation in MATLAB R2017a was used for the processing.

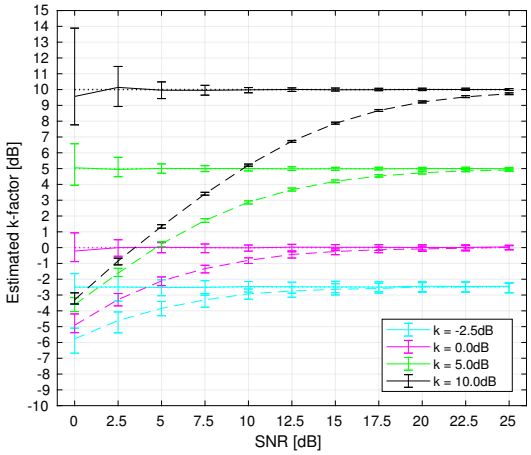

Fig. 6. Statistics of the estimated k-factors assuming known (solid lines) and unknown (dashed lines) noise levels in a simulated channel. The correct k-factors are shown with dotted lines.

In general terms, denoting $\mathrm{R}(\sigma_s, \sigma_r)$ as the Rice cumulative distribution function (CDF) and given a vector of measured amplitude samples, the parameters σ_s and σ_r are jointly optimized for best fit in the ML sense to the CDF of the data. When both $s_r(t)$ and $w(t)$ are random and present in measured data, the estimated $\tilde{\sigma}_r$ will approximate $\sqrt{\sigma_r^2 + \sigma_n^2}$ instead of the desired σ_r, since the noise component cannot be distinguished from the signal component. If we are able to estimate the noise power separately as $\tilde{\sigma}_n^2$ then a better approach is to optimize using the model CDF $\mathrm{R}(\sigma_s, \sqrt{\sigma_r^2 + \tilde{\sigma}_n^2})$ thus taking into account the random noise component.

The performances of the estimators are evaluated using simulated Rician channels assuming different k-factors and signal to noise ratios (SNRs). For each channel $2.5 \cdot 10^4$ samples are simulated and used for the ML estimation, with and without assuming a known noise level. Each estimation is repeated 100 times and Fig. 6 shows median values with 10% and 90% percentiles defining the error bars. It is noticed that the estimator not incorporating the noise level has an increasing bias when the SNR reduced, the other estimator gives the correct k-factor, at least in median. However, the variation seems to be small for SNRs above 5 dB.

In the processing of each measurement, the noise power was estimated as the average power in the impulse responses (IRs) for delays in the range 1.5–2.4 μs where any signal components are far below the noise floor. The average is over both delay and snapshots.

Narrow-band data is obtained from the IRs using discrete Fourier transforms (DFTs) and useful sub-channels were defined as those within 15 dB of the max average power. For each useful sub-channel the samples were normalized, and samples from all useful sub-channels were used as input to the ML estimation procedure, together with the estimated noise power. The number of samples used for the estimation is about $1.33 \cdot 10^5$

Accepted for *The 2018 IEEE 29th Annual International Symposium on Personal, Indoor and Mobile Radio Communications (PIMRC).*

to $1.58 \cdot 10^5$, depending on the measurement. Using the estimated Rice parameters, the k-factor was computed using (2).

In addition, the mean total power was computed as $P_{\text{tot}} = \sum_{n=1}^{N} \sum_{m=1}^{M} |h(n,m)|^2/M$ where $h(n,m)$ is the IR at delay index n and snapshot index m, and where $N = 960$ and $M = 525$ are, respectively, the number of samples in delay and space/time.

IV. Results

Fig. 7 shows the measured mean total power when using the omni-directional antenna at the different locations and environments. The individual results for the sub-locations and any repetitions are shown with crosses, with lines connecting the mean of the values at the same location. All values are normalized to the maximum power level observed at L19 in the Hall.

The orientation of the Tx antenna has a significant impact on the power in the Lab and Hall where a LOS exists. This variation is partly due to the radiation pattern of the Tx antenna, but this alone cannot explain the variations over locations, since the about 6 dB of difference in the Lab is less than what would be expected from the pattern. The importance of the LOS is also illustrated at L19–L24, where the power varies according to the location relative to the main beam of the Tx antenna.

Fig. 8 shows some examples of the CDFs for the measured and estimated Rice models. When the noise is not taken into account in the estimation, the power in the random part is overestimated, leading to the (dotted) CDFs closest to the measured curves. When including the noise in the estimation, the k-factor is effectively increased (dashed curves). It is noted that in either case the Rician model is not a perfect match to the measured data, perhaps with the near-Rayleigh case as an exception. The Rician model should be viewed as a simplification of the actual channel and the k-factors as indicators of the general type of channel measured. Better fitting models may exist, but is not explored further in this work. Other optimization goals (non-ML) may also be employed, e.g., for a better fit in the low-power CDF region.

An overview of the estimated Rician models is presented in Fig. 9 in the form of k-factors. The plots show the k-factors estimated at the different sub-locations and repetitions (when available), with lines connecting mean values. Curves are shown both for estimates taking into account measurement noise as well as for estimates obtained ignoring noise. As expected, the k-factor is highest when noise is considered, by about 0–1 dB, depending the location.

In the Lab and Hall environments the k-factor is highly dependent on whether or not the location is within or near the main beam of the Tx horn, with relatively high values in the range 2–9 dB, or low values in the range -10 to 0 dB outside the main direction.

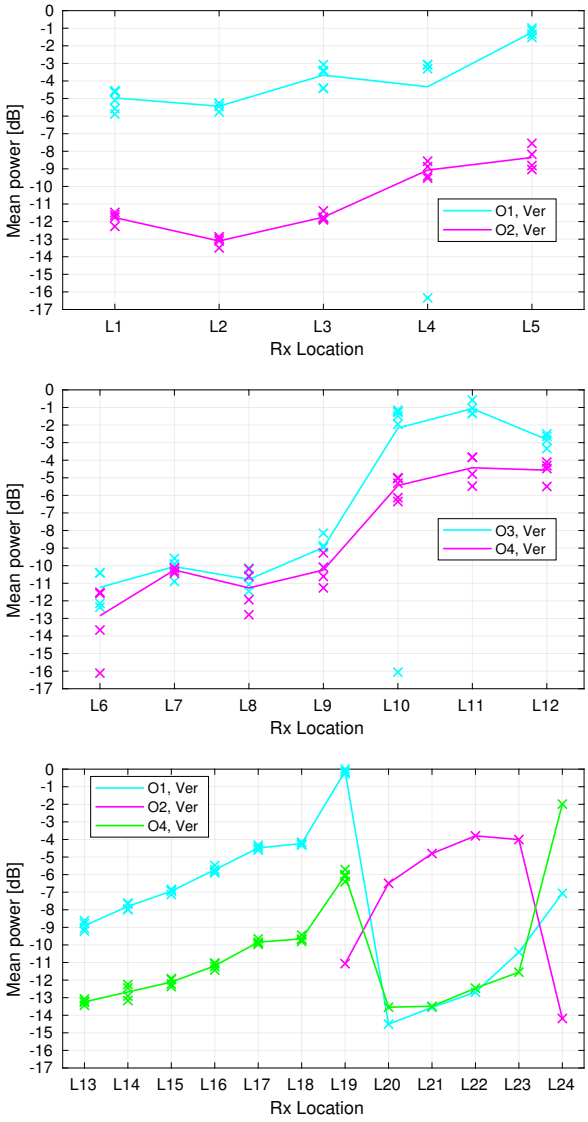

Fig. 7. Mean total power for different Tx antenna orientations and locations in the Lab (top), Corridor (middle), and Hall (bottom) environment. All values are normalized to the maximum observed in the Hall environment.

The k-factors in the Corr environment is generally below 2 dB, with the highest values in LOS conditions. The relatively low k-factors in LOS, compared to those in the Lab and Hall environments, may be partly due to the Rx being close to the Tx, so that the LOS is affected by elevation pattern due to the height difference. However, the power level at L10–L12 is in fact higher than that obtained at L20–L23, where the k-factors are in the range 6–8 dB.

Accepted for *The 2018 IEEE 29th Annual International Symposium on Personal, Indoor and Mobile Radio Communications (PIMRC).*

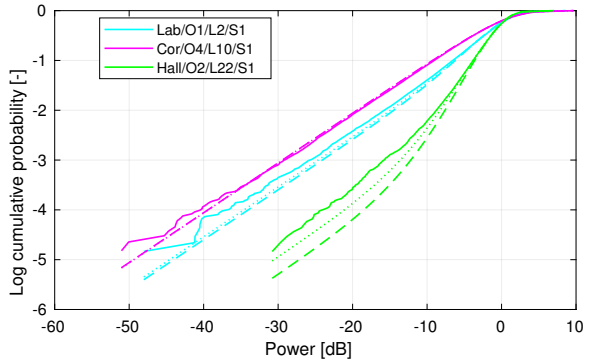

Fig. 8. Examples of estimated CDFs based on the measured amplitudes in all sub-channels. For each measured case Rician CDFs are also shown using the same color, where dashed-line CDFs are obtained using ML optimization taking into account the measurement noise and dotted-line CDFs are for optimization ignoring the noise.

V. Conclusions

Based on 26 GHz channel measurements at many indoor locations it was found that the mean power is strongly influenced by the presence of LOS and the radiation pattern of the AP, with variations up to 10 dB in one environment. Similarly, the orientation of the AP is important. Rician models were optimized to fit the measured narrowband amplitude data. The model fit is generally reasonable, but not perfect, with the best result for low k-factors. In two relatively large room environments the k-factor is highly dependent on the mobile unit being in the main beam of the AP antenna where values are in the range 2–9 dB. Elsewhere the k-factor is -10 to 0 dB. In a more confined corridor environment the k-factors are generally below 2 dB, even in LOS conditions.

Acknowledgments

The authors would like to thank Kim Olesen, Kristian Bank, and Johannes Hejselbæk for their assistance during the measurements.

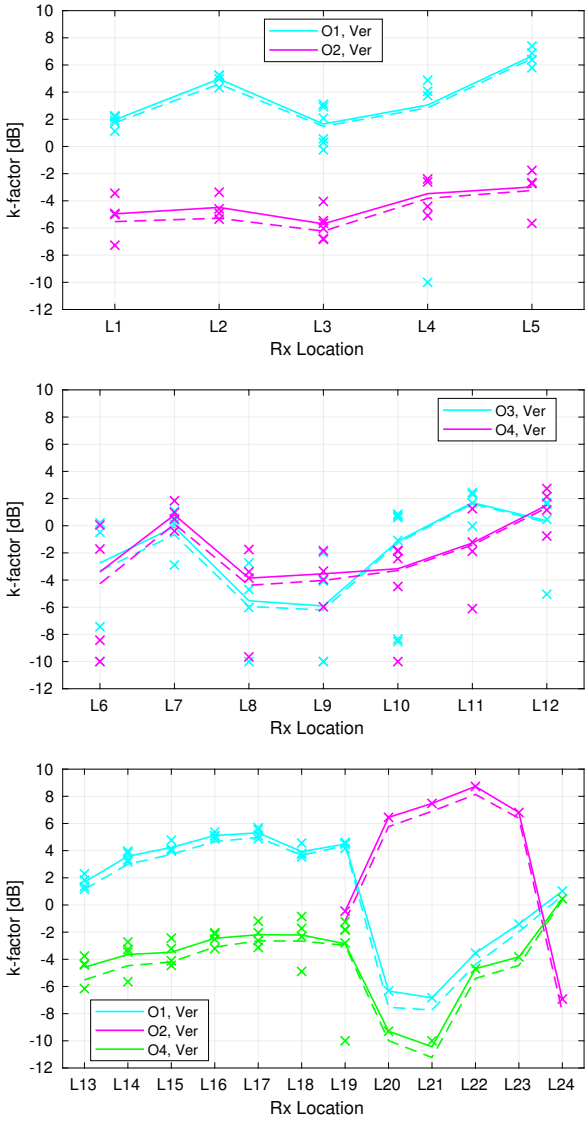

Fig. 9. Estimated k-factors for different locations in the Lab (top), Corridor (middle) and Hall (bottom) environment. The solid lines connect mean values of estimates taking into account the noise power, while dashed lines connects mean values of points (not shown) estimated ignoring the effects of noise.

References

[1] M. Samimi, K. Wang, Y. Azar, G. N. Wong, R. Mayzus, H. Zhao, J. K. Schulz, S. Sun, F. Gutierrez, and T. S. Rappaport, "28 GHz angle of arrival and angle of departure analysis for outdoor cellular communications using steerable beam antennas in new york city," in *Vehicular Technology Conference (VTC Spring), 2013 IEEE 77th*, June 2013, pp. 1–6.

[2] Y. Azar, G. N. Wong, K. Wang, R. Mayzus, J. K. Schulz, H. Zhao, F. Gutierrez, D. Hwang, and T. S. Rappaport, "28 GHz propagation measurements for outdoor cellular communications using steerable beam antennas in new york city," in *Communications (ICC), 2013 IEEE International Conference on*, June 2013, pp. 5143–5147.

[3] N. Iqbal, C. Schneider, J. Luo, D. Dupleich, R. Müller, S. Haefner, and R. S. Thomä, "On the stochastic and deterministic behavior of mmwave channels," in *11th European Conference on Antennas and Propagation (EUCAP)*, 2017, pp. 1813–1817.

[4] M. K. Samimi, G. R. MacCartney, S. Sun, and T. S. Rappaport, "28 GHz millimeter-wave ultrawideband small-scale fading models in wireless channels," in *83rd Vehicular Technology Conference (VTC Spring)*, May 2016, pp. 1–6.

[5] M.-T. Martinez-Ingles, J.-M. Molina-Garcia-Pardo, J.-V. Rodrguez, J. Pascual-Garca, and L. Juan-Llcer, "Experimental comparison between centimeter- and millimeter-wave ultrawideband radio channels," *Radio Science*, vol. 49, no. 6, pp. 450–458, 2014, 2014RS005439. [Online]. Available: http://dx.doi.org/10.1002/2014RS005439

[6] J. Ø. Nielsen and G. F. Pedersen, "Dual-polarized indoor propagation at 26 GHz," in *2016 IEEE 27th Annual International Symposium on Personal, Indoor, and Mobile Radio Communications (PIMRC)*, Sept 2016, pp. 1–6.

[7] R. Vaughan and J. B. Andersen, *Channels, propagation and antennas for mobile communications*. London, United Kingdom: The Institution of Electrical Engineers, 2003.

[8] J. Sijbers, A. J. den Dekker, P. Scheunders, and D. V. Dyck, "Maximum-likelihood estimation of Rician distribution parameters," *IEEE Trans. on Medical Imaging*, vol. 17, no. 3, pp. 357–361, June 1998.

Accepted for *The 2018 IEEE 29th Annual International Symposium on Personal, Indoor and Mobile Radio Communications (PIMRC).*